Chapter 4

Effect of Mechanical Milling on the Magnetic Properties of Garnets

4.1. Introduction

Rare earth iron garnets (RIG) have been extensively studied as they are an important class of ferrimagnetic materials because of their high frequency applications [1]. They have different crystallographic sites with 16 Fe^{3+} ions in the octahedral [a] sites, 24 Fe^{3+} ions in the tetrahedral (d) sites and 24 R^{3+} in the dodecahedral {c} sites. The magnetic contribution arises from the antiparallel alignment of the rare earth magnetic moments in the {c} site to the resultant of the antiparallely coupled magnetic moments in the other two sites having Fe^{3+} ions. The net magnetization direction at 0 K is determined by the {c} sublattice magnetization due to its large magnetization at low temperatures. At high temperatures, the weak coupling between the magnetic moments decreases the magnetization of the {c} sublattice rapidly. At the compensation temperature (T_{comp}), the {c} sublattice magnetization is equal and opposite to the resultant of the [a] and (d) sublattice magnetizations. The compensation temperature of gadolinium iron garnet (GdIG) is 290 K [2].

Even though sintering is done at a high temperature of 1573 K during the synthesis of garnets [3], a small amount of orthoferrite phase is generally found to be present as an impurity phase [4]. Efforts have been made to lower the calcination temperature by milling the precursor oxides [5]. It has been observed in ferrites that the reduction of grain size gives rise to changes in cation distribution, magnetization and Néel temperature [6-8]. However, to the best of our knowledge, there has been no report on the study of the magnetic properties of the GdIG with nanometer grain sizes. Hence, it is interesting to study the effect of grain size on the structural and magnetic properties of the garnets [9]. In this chapter, the changes in the phase stability and magnetic properties of yttrium and gadolinium iron garnets subjected to milling are studied.

4. 2.   Experiment

For our study, as-prepared yttrium and gadolinium iron garnets obtained from the sintered blocks were ball-milled in a Fritsch planetary high-energy ball mill (P7) in air. Zirconia balls and vials were used for milling with a ball to weight ratio of 10:1 at a milling speed of 600 rpm. The milled samples were sampled out at different milling times. X-ray diffraction measurements were performed using a Cu or Fe target. The average grain size was calculated using the Scherrer formula. The magnetic measurements were done using a vibrating sample magnetometer (VSM) (EG&G, PARC, USA) in fields up to 560 kA/m and with a quantum design SQUID magnetometer for fields up to 5.6 MA/m at various temperatures with a stability of ± 5 K. The Mössbauer measurements were performed using a constant acceleration Mössbauer spectrometer (Wiessel, Germany) at 300 K and at 16 K with a ^{57}Co/Rh radioactive source kept at 300 K.

4. 3.   Results and Discussion

4.3.1. Structure and magnetic properties of yttrium iron garnet on milling

Figure 4.1. shows the XRD patterns of the as-prepared and ball-milled yttrium iron garnet (YIG).   It is seen from the XRD patterns that the YIG decomposes to $YFeO_3$ and α-Fe_2O_3 on milling. The grain size of YIG is found to decrease from 91 nm for the as-prepared sample to 20 nm on milling to 15 h. Figure 4.2 shows the Mössbauer spectra of the YIG at 300 K for the as-prepared and the 5 h milled samples. The
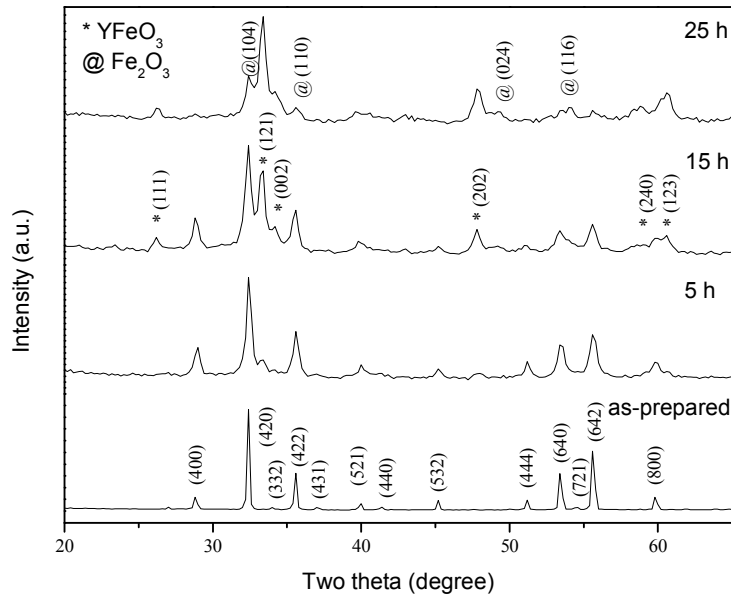
Fig. 4.1. The XRD (Cu-target) patterns of yttrium iron garnet ball-milled for various durations.

Mössbauer spectrum for the as-prepared sample shows two sextets corresponding to Fe^{3+} ion in tetrahedral and octahedral sites. However, when the YIG is milled for 5 h, a doublet also appears in the Mössbauer spectrum. The presence of the doublet indicates that some of the particles are superparamagnetic at 300 K. Figure 4.3 shows the magnetization and coercivity at 300 and 77 K for the YIG samples milled for various durations. The magnetization at both temperatures shows a decreasing trend with milling, which could be due to the appearance of the antiferromagnetic phases like $YFeO_3$ and α-Fe_2O_3. With milling, the coercivity at 77 K increases whereas at
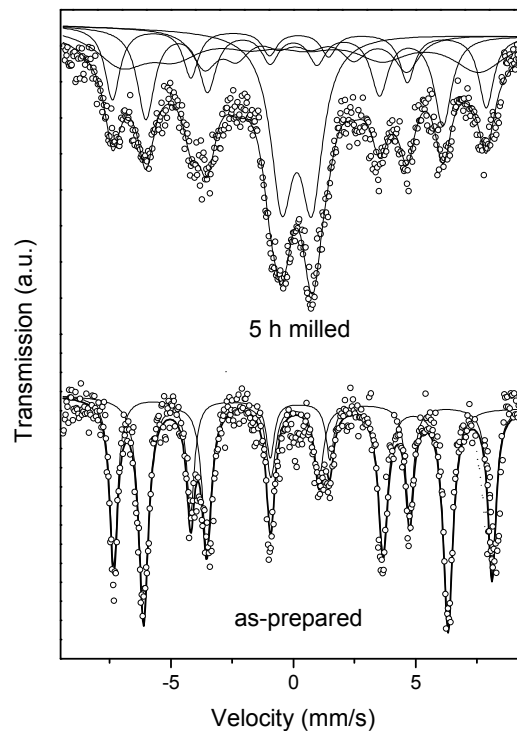
Fig. 4.2. The Mössbauer spectra at 300 K for the as-prepared and the 5 h milled YIG.
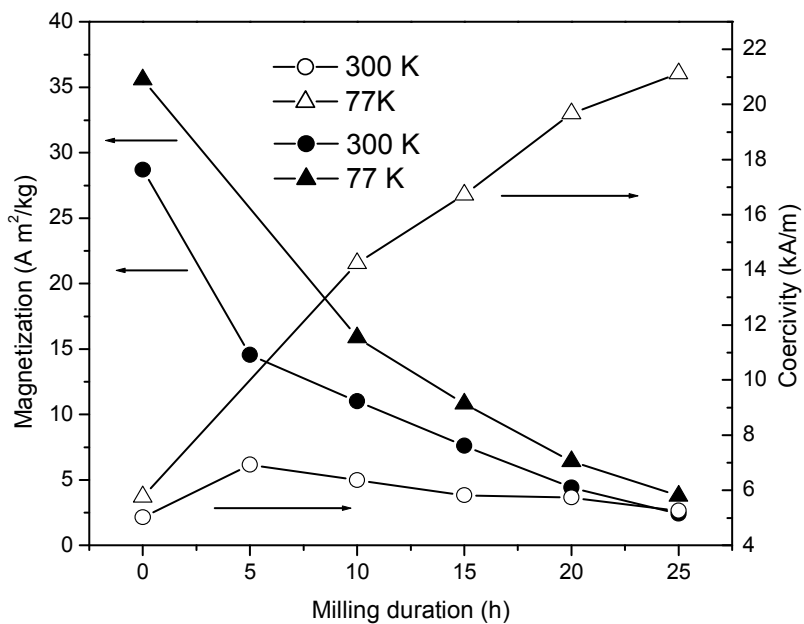
Fig. 4.3. The magnetization and coercivity of yttrium iron garnet at 300 and 77 K for various milling durations. (The continuous lines are guide to the eye).

300 K it decreases. The calculated single domain size for the YIG is 300 nm and the maximum coercivity has been reported for the 200 nm particles [10]. Since the grain sizes of the milled samples in the present study are below the single domain size, as observed from the appearance of superparamagnetic doublet in the Mössbauer spectrum shown in Fig. 4.2, the coercivity is expected to decrease with further grain size reduction. However, the increase in coercivity at 77 K with milling may be due to the increase in the surface anisotropy for smaller particles. The coercivity at 300 K increases with milling up to 5 h due to the increase in the effective magnetic anisotropy due to the strain introduced and then decreases with further milling due to the increase in the volume fraction of small particles which are superparamagnetic at this temperature. At 300 K, the decrease in coercivity due to superparamagnetism should be predominant over the increase due to the surface anisotropy and it should be other way at 77 K to explain the observed results.

4.3.2. Gadolinium iron garnet

4.3.2.1. X-ray diffraction studies

Figure 4.4 shows the XRD pattern of the gadolinium iron garnet (GdIG) milled for
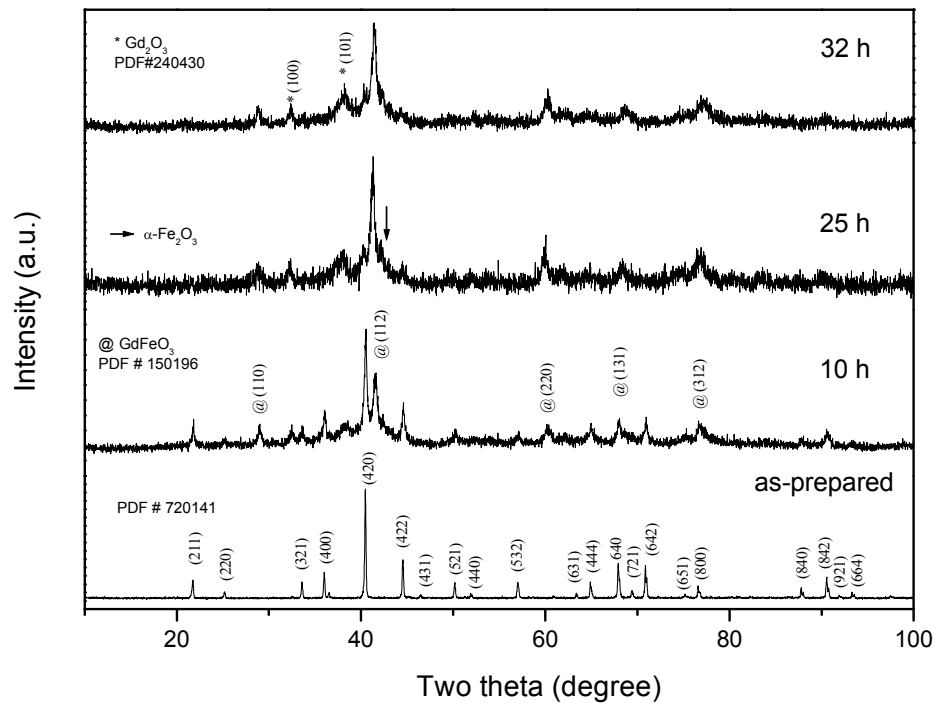
Fig. 4.4. The XRD pattern (Fe-target) of the GdIG ball-milled for various durations.

various durations. The GdIG phase decomposes into $GdFeO_3$, Gd_2O_3 and α-Fe_2O_3 on milling. The average grain size for the GdIG phase is reduced with milling from 78 nm for the as-prepared to 33, 23 and 16 nm for the 10, 25 and 32 h milled samples respectively. The volume fraction of the GdIG phase is found to decrease with milling time. However, a quantitative analysis of the intensity of the phases is not easy because of the line broadening and overlapping of the most intense peak of the α-Fe_2O_3 phase with its $GdFeO_3$ phase counterpart.

4.3.2.2. Magnetic properties

Figure 4.5.(a) shows the first quadrant hysteresis loops at 77 K for the as-prepared and milled GdIG samples. The magnetization at 77 K decreases with milling due to the increase in the volume fraction of the antiferromagnetic and non magnetic phases on milling. Figure 4.5.(b) shows the first quadrant hysteresis loops at 300 K of the as-prepared and the milled samples of GdIG. Figure 4.5.(c) shows the magnetization at 300 and 77 K for the GdIG milled for various durations. It is seen that the magnetization at 300 K increases from 1.1 A m^2/kg for the as-prepared sample to 5.1 A m^2/kg on milling for 25 h
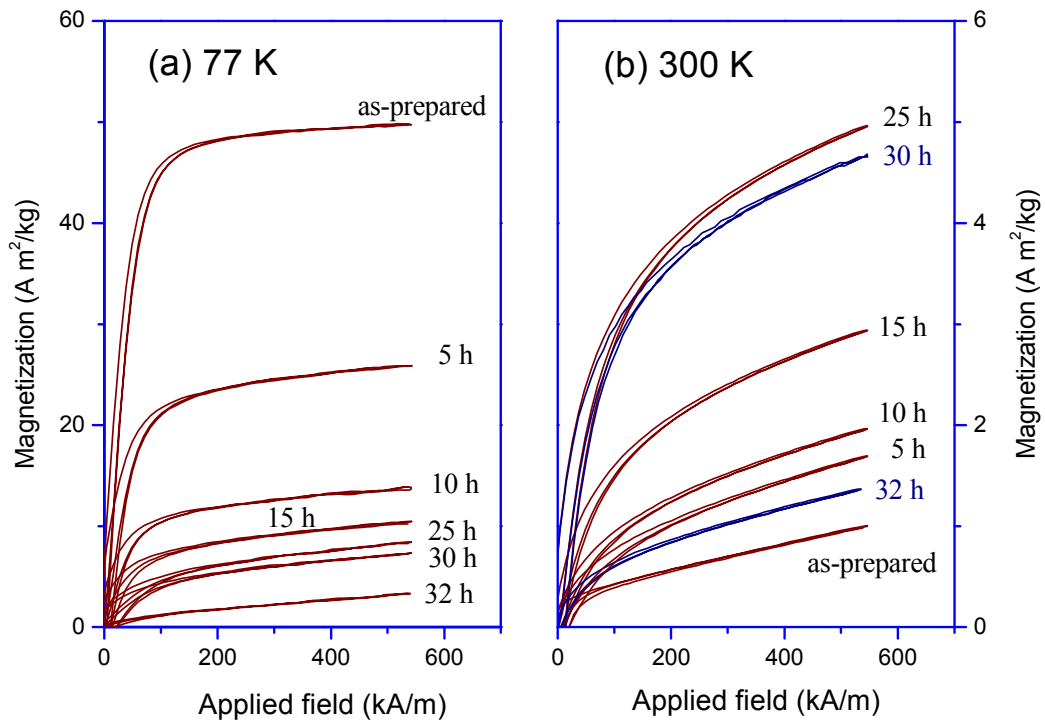
Fig. 4.5. The first quadrant hysteresis loops at **(a)** 77 K and **(b)** 300 K of GdIG milled for various durations.
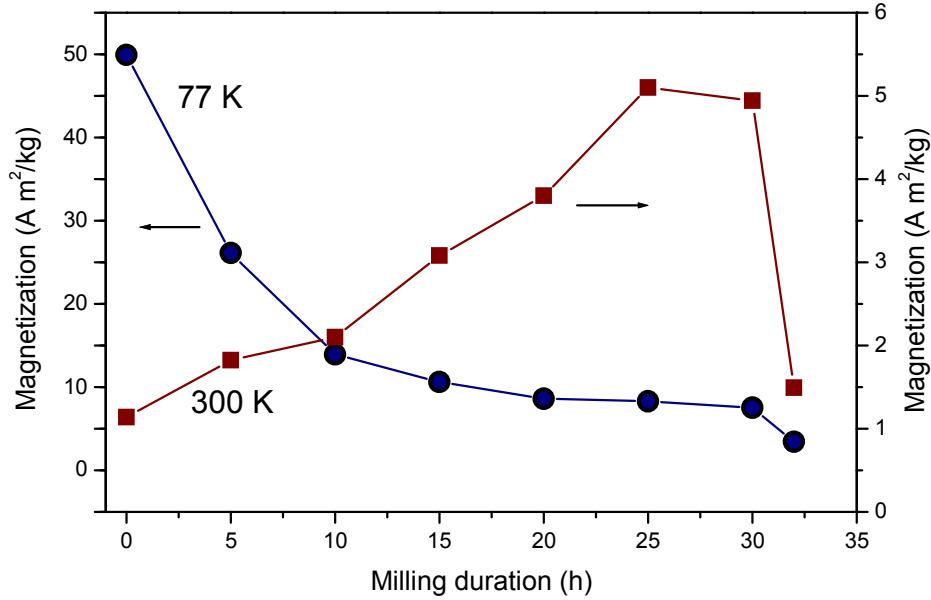
Fig. 4.5. (c) The magnetization at 300 and 77 K for the GdIG milled for various durations.(The continuous lines are guide to the eye).

but decreases upon further milling beyond 25 h to 1.5 A m^2/kg for the 32 h milled samples. The decrease, for 32 h milling, arises from the formation of a large volume fraction of the antiferromagnetic oxides as revealed by XRD and also due to surface effects [11]. The increase in the magnetization at 300 K up to 25 h of milling, inspite of the presence of antiferromagnetic and non-magnetic phases, could be attributed to the lowering of the T_{comp} on milling as discussed in Section 4.3.2.2.(a).

4.3.2.2.(a) Effect of milling on the compensation temperature of GdIG

The compensation temperature for the as-prepared GdIG is observed to be 290 K which is found to vary according to the relation [12]

$$T_{comp} = g\mu_B^2 \frac{N_A(S+1)}{3k}(\lambda_{aa} + \lambda_{ad})M_a(0) \tag{4.1}$$

with

$$(\lambda_{aa}+\lambda_{ad})\, M_a(0) = (\lambda_{dd}+\lambda_{ad})\, M_d(0)$$

where λ_{aa}, λ_{ad}, λ_{dd} are the molecular field coefficients of sublattices *aa*, *ad* and *dd* respectively and $M_a(0)$ and $M_d(0)$ are respectively the [a] and (d) sublattice magnetizations
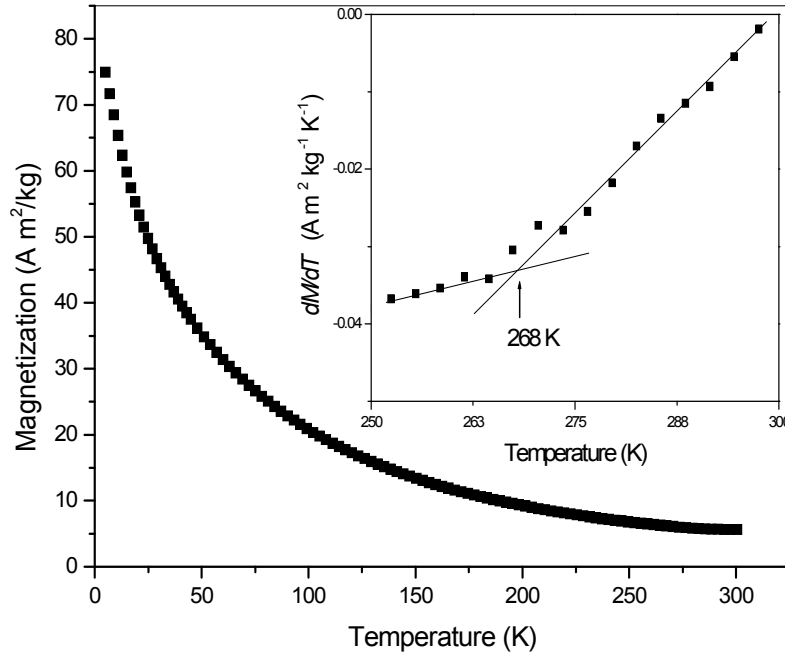
Fig. 4.6. The magnetization vs. temperature curve of the 10 h milled GdIG in an applied field of 4 MA/m. The inset shows *dM/dT* with temperature.

at 0 K. The superexchange interaction strength between various sites is determined by the cation-oxygen-cation bond angle in the two sublattices with the maximum occurring for an angle of 180 $^{\circ}$. In GdIG, the Fe^{3+}[a] - O^{2-} - Fe^{3+}[a] bond angle is 147.2 $^{\circ}$ and the Fe^{3+}[a] - O^{2-} - Fe^{3+}(d) and Fe^{3+}(d) - O^{2-} - Gd^{3+}{c} bond angles being 127.4 $^{\circ}$ and 121.4 $^{\circ}$ respectively. The other bond angles such as Fe^{3+}(d) - O^{2-} - Fe^{3+}(d), Gd^{3+}{c} - O^{2-} - Gd^{3+}{c} etc. are still smaller and hence these bonds are weaker [1]. The mechanical milling not only introduces defects and oxygen vacancies but also could modify the bond angle as reported in the literature [13].

The oxygen vacancies introduced an a possible decrease in bond angle due to mechanical milling will decrease the superexchange interaction strength and hence the values of λ_{aa} and λ_{ad} leading to a decrease in the compensation temperature. Figure 4.6 shows the variation of magnetization with temperature for the 10 h milled GdIG in an applied field of 4 MA/m and the inset shows the differential change in the magnetization
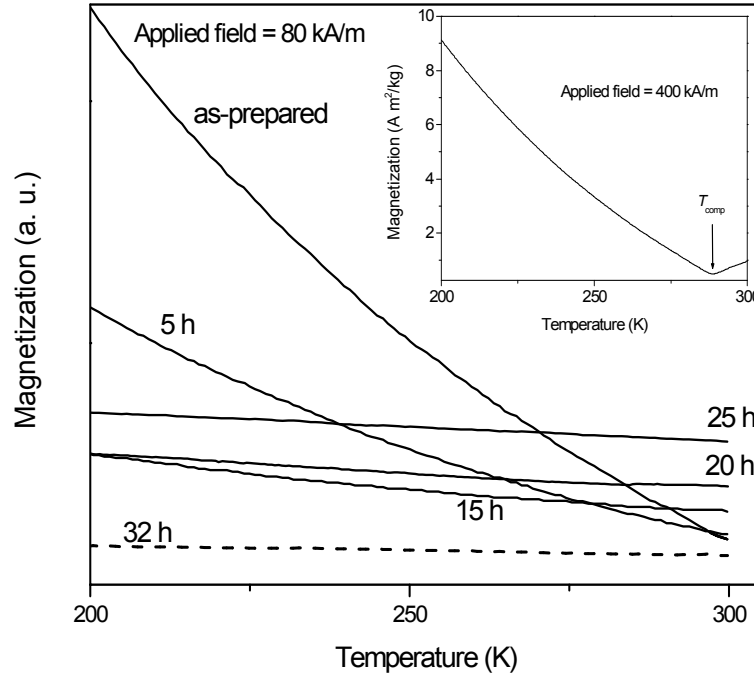
Fig. 4.7. The thermomagnetization curves of the as-prepared and milled GdIG in an applied magnetic field of 80 kA/m. The inset shows the T_{comp} of the as-prepared GdIG in an applied field of 400 kA/m.

with temperature. The slope of the *dM/dT* vs. *T* plot changes at a temperature of 268 K and this temperature is the compensation temperature T_{comp}.

Figure 4.7 shows the thermomagnetization curves of the GdIG at 80 kA/m for the samples milled for various durations. We could observe that the thermomagnetization curves of the milled samples crosses that of the as-prepared one, with the point of intersection shifting to lower temperatures with increase in milling duration. Figure 4.8 shows the crossing temperature of the magnetization curves of the samples milled for different durations. The crossing occurs at 296 K for the 5 h milled sample, which decreases to 270 K for the 25 h milled sample. The decrease in the crossing temperature shows that the compensation temperature decreases with milling. This indicates that the superexchange interaction in the Gd ion sublattice has weakened with milling. This weakening could arise due to defects which cause the bond angles to change and also due to the breaking of superexchange bonds because of the loss of oxygen ions on milling as indicated by the Mössbauer studies described in Section 4.3.2.3.

At 300 K, an increase in the magnetization is clearly seen, from Fig. 4.7, for the samples milled up to 25 h and this is attributed to the decrease in T_{comp} with milling due to the uncompensated moments of the sublattices caused by the weakening of the superexchange interaction whereas the as-prepared GdIG shows a T_{comp} of 288 K as seen from the thermomagnetization plot shown in the inset of Fig. 4.7.
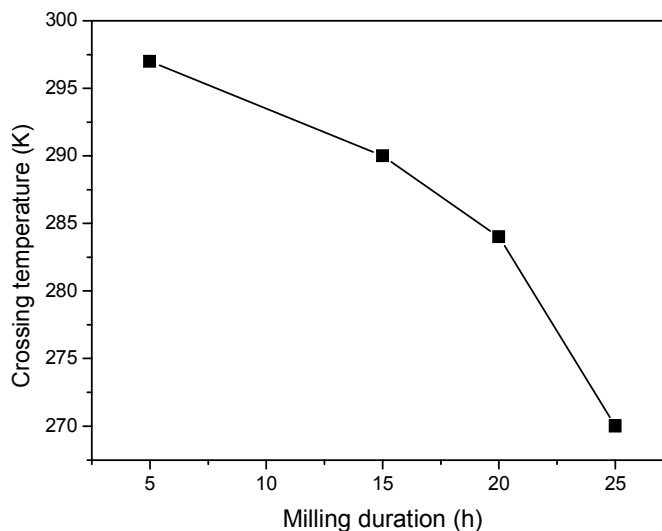
Fig. 4.8. The crossing temperature of the GdIG milled for various durations.

The 32 h milled sample shows a significantly smaller magnetization in the range from 200 to 300 K as compared to the samples milled for smaller durations. This is because of the presence of a relatively large volume fraction of the antiferromagnetic and non-magnetic phases as revealed by XRD.

4.3.2.2.(b) Canted spin structure

Figure 4.9 shows the magnetization curves for the as-prepared GdIG at 5 K and for the 10 h milled samples at various temperatures. We could observe that at 5 K, the saturation is easily obtained even at a smaller field of 560 kA/m for the as-prepared sample, whereas the magnetic saturation is not obtained even at the highest available applied field of 5.6 MA/m for the 10 h milled sample. The instauration of the loop suggests the presence of the canted spin structure in the milled samples. The canted spin structure could arise due to the weakening of the superexchange interaction on mechanical milling which causes structural damages and introduces defects. The canted spin structure is linked to the effective anisotropy, K_{eff} which increases because of the introduction of lattice strains on milling and also due to the surface spin effects of the small particles. In $Gd_3Fe_5O_{12}$, both Gd^{3+} and Fe^{3+} ions are in the S state and hence their contribution to cubic anisotropy is not significant. Therefore, the presence of anisotropy in the nanoparticles of GdIG could be arising out of surface contributions. The magnetization curve does not saturate to allow the
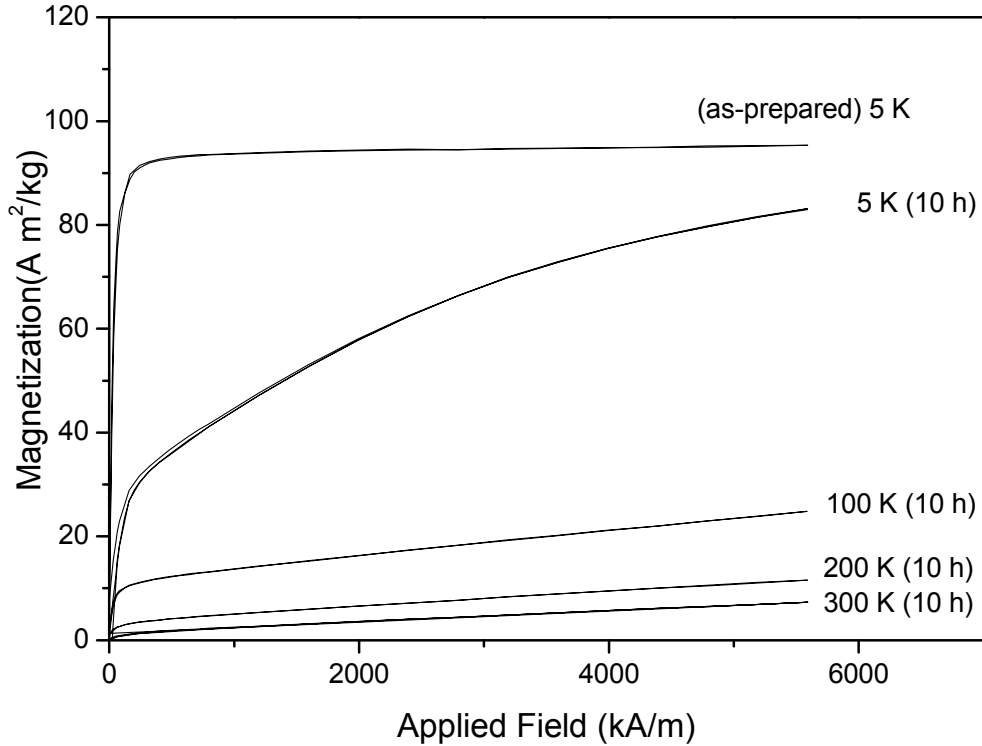
Fig. 4.9. The first quadrant hysteresis loops recorded at 5 K for the as-prepared GdIG and at various temperatures for the GdIG milled for 10 h.

extrapolation of M_s at zero field and the behaviour of the curve above 7 T is unknown in our case. As a first approximation, one could take the value of M_s at 7 T as the value of spontaneous magnetic moment. This value of 83 A m^2/kg for the 10 h milled sample is found to be smaller than the value of 95 A m^2/kg for the as-prepared sample. But it is to be remembered that in the milled samples, antiferromagnetic phases are present as indicated by XRD. It is possible to estimate, to a first approximation, that the relative volume percentage of these phases is not less than 25 %. Taking into account of the presence of the antiferromagnetic phases, the actual magnetization turns out to be 104 A m^2/kg and this increase can be attributed to canting of moments in the milled sample. The canting also may be responsible for the observed increase in the magnetization at 300 K in addition to the decrease in T_{comp} with milling. For the 25 h milled samples we could not obtain sufficient saturation to analyse the result.

4.3.2.2.(c) Effect of milling on the coercivity

Figure 4.10 shows the coercivity at 300 and 77 K of the as-prepared and GdIG milled for various durations. The coercivity at 300 K for the as-prepared GdIG is 16.4 kA/m which decreases to 8.2 kA/m for milling up to 32 h whereas the coercivity at 77 K increases from 5.3 kA/m for the as-prepared to 21.1 kA/m on milling up to 25 h and decreases to 14 kA/m on further milling to 32 h. The coercivity of the as-prepared GdIG at 77 K is 5.3 kA/m whereas at 300 K it is 16.4 kA/m. Since the coercivity $H_c = 2K/M_s$, where K is the anisotropy constant and M_s is the saturation magnetization, the increase in the M_s value at 77 K compared to that at 300 K, as seen from Fig. 4.5.(c) decreases the coercivity of the as-prepared GdIG at 77 K. The coercivity at 300 K decreases for milling up to 15 h and then increases up to 25 h. This could be explained based on the combined effect of superparamagnetism and the increasing surface anisotropy with milling. At 77 K, the increase in the coercivity with milling may be due to the increase in the surface anisotropy of small particles as described in Section 4.3.1. The decrease in coercivity for the 32 h milled sample may be due to the decrease in the grain size to 16 nm.
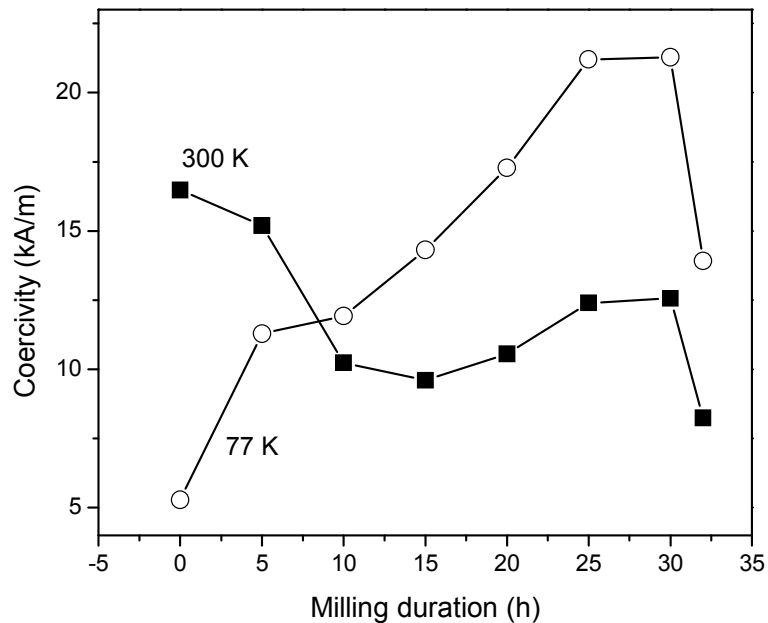
Fig. 4.10. The coercivity at 300 and 77 K of GdIG milled for various durations.

4.3.2.3. Mössbauer studies

Figure 4.11.(a) shows the Mössbauer spectrum of the as-prepared GdIG at 300 K. The dots represent the experimental spectrum and the continuous curve results from the least-squares fitting of the experimental data. The ratio of the intensities of the peaks in a sextet was fixed as 3:2:1:1:2:3 assuming random orientation of grains in polycrystalline samples. The relative intensity of the Mössbauer spectra of the octahedral and tetrahedral sites of the GdIG is fixed to the ratio of their site population as 2:3. Figure 4.11.(b) gives the Mössbauer spectrum at 300 K for the GdIG milled for 10 h. The relative intensities of the various sextets were iterated. The sextet with a large quadrupole splitting is assigned to α-Fe_2O_3. The fitted parameters are given in Table 4.1. The Mössbauer spectra arising from ^{57}Fe in octahedral [a] and tetrahedral (d) sites are easily distinguishable for the as-prepared GdIG because of the large difference in their hyperfine fields of 49.0 and 40.2 T respectively. On milling the as-prepared GdIG for 10 h, a superparamagnetic doublet with a large linewidth is obtained along with four sextets arising from the [a] and (d) sites of GdIG, $GdFeO_3$ and α-Fe_2O_3. The correlation of the hyperfine fields to the various crystalline phases is difficult because of the reduced hyperfine fields due to superparamagnetism of small particles. However, in the absence of superparamagnetism, the hyperfine fields were found to be in the order of H_{hf}(octa) > H_{hf}($GdFeO_3$) > H_{hf}(α-Fe_2O_3) > H_{hf}(tetra) [14-16]. The co-existence of the doublet with the sextets is because of the distribution in the particle size, the smaller particles exhibiting superparamagnetism at 300 K. The reduction in the magnitude of the hyperfine fields on milling is due to the relaxation effects and also because of the surface spins of the small particles. Figure 4.12 shows the Mössbauer spectra of the as-prepared, 10 h, 25 h and 30 h milled samples at 16 K . The relative intensities of the various sextets were iterated while the relative intensities of the spectra for the octahedral and tetrahedral sites of GdIG were constrained to the ratio 2:3. The Mössbauer parameters are listed in Table 4.1. The absence of the superparamagnetic doublet at 16 K indicates that the measurement temperature is lower than the blocking temperature of the particles. For the as-prepared GdIG, the hyperfine magnetic field increased to 54.7 T for the octahedral site and to 48.2 T for the tetrahedral site at 16 K which is in accordance with the values reported by Cook and Li [15].
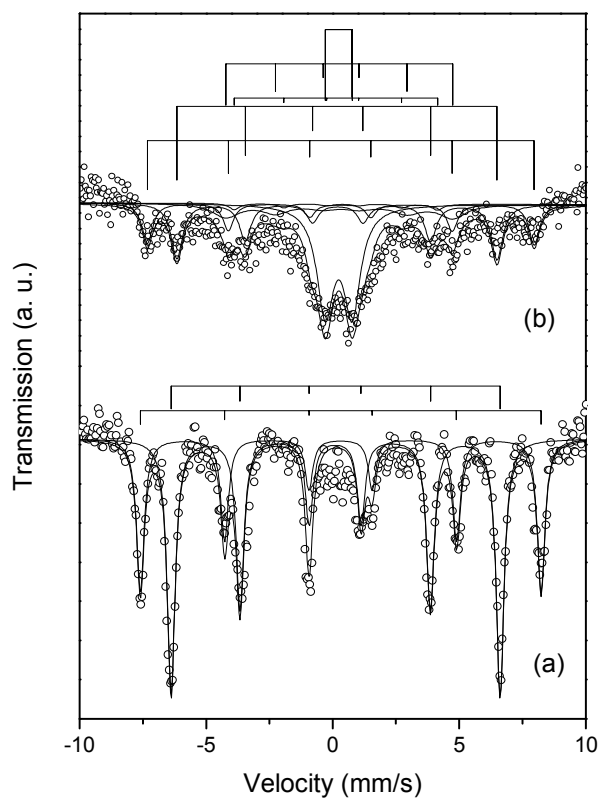
Fig. 4.11. The Mössbauer spectrum at 300 K for the **(a)** as-prepared and **(b)** 10 h milled GdIG.
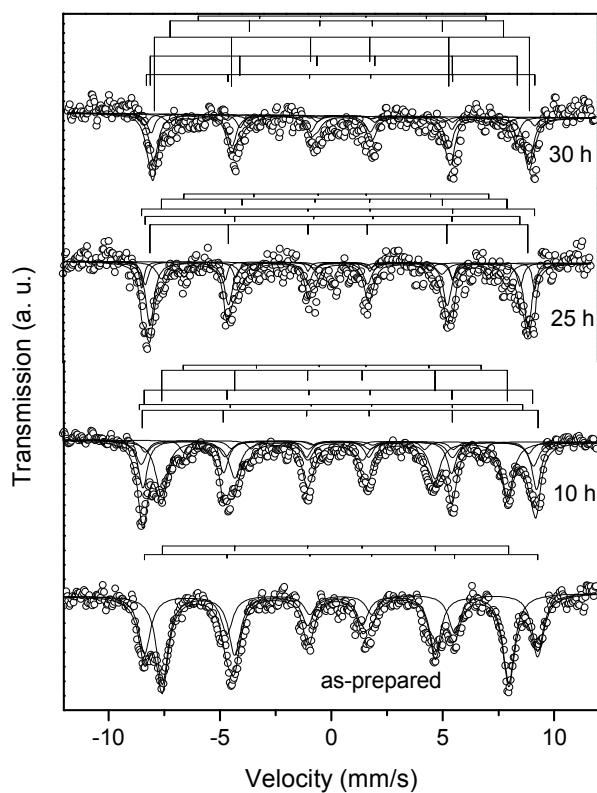
Fig. 4.12. The Mössbauer spectra at 16 K of the GdIG milled for various durations.

Table 4.1. The Mössbauer parameters of the as-prepared and the milled GdIG.

Sample details and measurement temperature	Hyperfine field ($\pm$ 0.1 T)	Isomer shift* ($\pm$ 0.05 mm/s)	Quadrupole splitting ($\pm$ 0.06 mm/s)	Line width ($\pm$ 0.05 mm/s)	Relative Intensity ($\pm$ 1%)	Phase/site
As-prepared 300 K	49.0	0.43	0.01	0.39	40	octa
	40.2	0.22	-0.02	0.36	60	tetra
10 h milled 300 K	47.3	0.42	0.02	0.49	18	A1
	39.1	0.30	0.04	0.54	27	A2
	27.8	0.41	0.08	1.27	15	A3
	24.9	0.37	0.28	0.50	03	A4
	-	0.24	1.06	0.80	37	superpara
As-prepared 16 K	54.7	0.55	0.02	0.64	40	octa
	48.2	0.29	-0.03	0.63	60	tetra
10 h milled 16 K	54.7	0.45	0.09	0.48	28	octa
	48.0	0.27	0.03	0.63	42	tetra
	54.5	0.42	0.07	0.58	17	$GdFeO_3$
	53.2	0.49	0.25	0.48	07	$\alpha\text{-}Fe_2O_3$
	41.6	0.32	0.20	0.41	06	unidentified
25 h milled 16 K	54.6	0.47	0.04	0.24	11	octa
	47.9	0.47	0.35	0.56	17	tetra
	52.5	0.46	0.05	0.45	50	$GdFeO_3$
	52.1	0.45	0.52	0.35	14	$\alpha\text{-}Fe_2O_3$
	42.4	0.51	0.24	0.36	08	unidentified
30 h milled 16 K	53.9	0.56	0.02	0.37	08	octa
	46.4	0.60	0.42	0.57	12	tetra
	52.1	0.58	-0.04	0.49	58	$GdFeO_3$
	50.8	0.54	0.55	0.39	19	$\alpha\text{-}Fe_2O_3$
	40.4	0.65	0.31	0.57	03	unidentified

* relative to α-Fe at 300 K.

A1 to A4 phases are difficult to identify.

For the 10 h milled sample, the Mössbauer spectrum was fitted with five sextets. The two sextets corresponding to the octahedral and tetrahedral sites of the garnet phase with the intensity ratio of 2:3 showed the hyperfine fields of 54.7 and 48.0 T respectively. The sextet with a hyperfine field of 54.5 T and a small quadrupole splitting of 0.07 mm/s arises from $GdFeO_3$ which is cubic in structure. The sextet with a hyperfine field of 53.2 T

[16] and a quadrupole splitting of 0.49 mm/s arises due to α-Fe_2O_3. An unidentified sextet with a smaller hyperfine field of 41.6 T is also observed with a small relative intensity of about 6 %. It cannot be correlated to any impurity phase as it is not confirmed by the X-ray diffraction. It should, therefore, be due to ^{57}Fe with an environment quite different from that in the regular octahedral or tetrahedral site of the garnet phase. The Fe^{3+} ions on the surface of small particles with lower coordination might have given rise to this sextet with a smaller hyperfine field.

The Mössbauer spectra for GdIG milled for 25 and 30 h have similar features as that of the 10 h milled sample except that the relative intensities of the orthoferrite and α-Fe_2O_3 phases increase with milling duration. However, the hyperfine field values of the 30 h milled sample are slightly smaller and the isomer shifts are slightly more positive than that for the samples milled for 10 and 25 h. The loss of oxygen during milling might have reduced some of the Fe^{3+} ions to Fe^{2+} ions giving rise to higher values for the isomer shift and smaller values for the hyperfine fields.

4.4. Conclusion

As-prepared garnets, on milling, are found to decompose into rare earth orthoferrite and other oxides of rare earth and iron. The coercivity of the garnets at 77 K increases with milling due to the increase in the surface anisotropy of small particles. The magnetization at 300 K decreases for the yttrium iron garnet with milling whereas it increases in the case of gadolinium iron garnet for milling up to 25 h. The increase in magnetization in the latter case is attributed to the uncompensated moments of the sublattices caused by the weakening of the superexchange interaction. The defects introduced on mechanical milling and the breaking up of the superexchange bonds as a result of oxygen vacancies introduced by milling may weaken the superexchange interaction and lower the compensation temperature. The Mössbauer parameters give an indication for the loss of oxygen on milling.

References

[1]   G. Winkler, *Magnetic Garnets* (Friedr. Vieweg & Sohn, Braunschweig, 1981) Chap. 2.

[2]   S. Chikazumi, *Physics of Magnetism* (Wiley, New York, 1964) Chap. 5.

[3]   R. J. Young, T. B. Wu, and I. N. Lin, J. Mater. Sci. **25** (1990) 3566.

[4]   M. Ristić, I. Nowik, S. Popović, I. Felner, and S. Musić, Mater. Lett. **57** (2003) 2584.

[5]   L. B. Kong, J. Ma, and H. Huang, Mater. Lett. **56** (2002) 344.

[6]   C. N. Chinnasamy, A. Narayanasamy, N. Ponpandian, K. Chattopadhyay, H. Guerault, and J.-M. Greneche, J. Phys.: Condens. Matter **12** (2000) 7795.

[7]   C. N. Chinnasamy, A. Narayanasamy, N. Ponpandian, K. Chattopadhyay, K. Shinoda, B. Jeyadevan, K. Tohji, K. Nakatsuka, T. Furubayashi, and I. Nakatani, Phys. Rev. B **63** (2001) 184108.

[8]   C. N. Chinnasamy, A. Narayanasamy, N. Ponpandian, R. Justin Joseyphus, B. Jeyadevan, K. Tohji, and K. Chattopadhyay, J. Magn. Magn. Mater. **238** (2002) 281.

[9]   R. Justin Joseyphus, A. Narayanasamy, N. Sivakumar, M. Guyot, R. Krishnan, N. Ponpandian, and K. Chattopadhyay, J. Magn. Magn. Mater. **272-276** (2004) 2257.

[10] P. Vaqueiro, M. A. López-Quintela, J. Rivas, and J.-M. Greneche, J. Magn. Magn. Mater. **169** (1997) 56.

[11] R. H. Kodama, A. E. Berkowitz, E. J. McNiff Jr., and S. Foner, J. Appl. Phys. **81** (1997) 5552.

[12] P. Gornet and C. G. D'ambly, Phys. stat. sol. (a) **29** (1975) 95.

[13] V. Šepelak, U. Steinike, D. Chr. Uecker, S. Wißmann, and K. D. Becker, J. Sol. State. Chem. **135** (1998) 52.

[14] N. N. Greenwood and T. C. Gibb, *Mössbauer Spectroscopy*, (Chapman and Hall, London, 1971) Chap.10.

[15] D. C. Cook and J. Li, Hyper. Inter. **28** (1986) 495.

[16] W. Kundig, H. Bommel, G. Constabaris, and R. H. Lindquist, Phys. Rev. **142** (1966) 327.